Design of Saliency-Based Sensorless Controlled IPMSM with Concentrated Winding for EV Traction

Myung-Seop Lim[1], Seung-Hee Chai[1], and Jung-Pyo Hong[1], *Senior Member, IEEE*

[1]Department of Automotive Engineering, Hanyang University, Seoul 133-791, Korea

This paper investigates the influence of the geometry design parameters of saliency-based sensorless-controlled interior permanent magnet synchronous motors (IPMSMs) with concentrated winding on the sensorless drive feasibility. To evaluate the sensorless controllability of the motors, two different methods to estimate rotor position error are proposed. By using the methods, the geometry design parameters in the stator are analyzed to figure out which ones have a positive effect on sensorless drive. Based on the analysis result, in the full paper, a final model applied with a selected design parameter is going to be proposed for electric vehicle (EV) traction application. The validity of the proposed estimation methods and the design results will be verified by the experiments.

***Index Terms*—Inductance, permanent magnet motors, sensorless control, total harmonic distortion, traction motors**

I. Introduction

TODAY, an interior permanent magnet synchronous motor (IPMSM) is usually employed as electric vehicle (EV) traction because of its high torque density. To achieve the best performance of the machine, a position sensor is essential. However, this increases system cost, volume and complexity, and decreases reliability of the machine. In addition, the sensors are not durable enough to operate normally under severe environment conditions in vehicles. This concern is coming to the fore because if the sensors are in default, the driver cannot control the vehicle which will result in an accident. For these reasons, a design method of a sensorless-controlled motor is critical goal not only for system cost and volume reduction but also for fault-tolerant control feasibility.

Speed-dependent back electromotive force (BEMF) based sensorless control cannot be used in the zero- and low-speed ranges, because the magnitude of BEMF is extremely small. Therefore, based on saliency, the rotor position can be estimated by measuring the current inductance responses with high-frequency voltage injection [1]. It is not easy to estimate the rotor position under heavy load conditions, though, because the responses are distorted by the input current or the saturations [2], [3]. However, there are only a few design methods using the *q*-axis path optimization of the rotor [4], [5]. It is hard to find prior researches on the stator design methods. The advantages of applying the design parameters to a stator compared with a rotor are presented in [6].

In this study, basic principle of the saliency-based sensorless control and the cause of the occurrence of the estimation error are discussed. As a result, the two methods are proposed to estimate rotor position. First method is contour plotting of the *d*, *q*-axis inductance varied with rotor position, and second method is evaluating the total harmonic distortion (THD) of the phase inductances. By using the proposed methods, the influence of the design parameters in the stator such as closed slot, chamfer, and notch on the sensorless control feasibility is analyzed. Thus, the goal of this study is to propose the design method of the stator for concentrated winding sensorless-oriented machines that can be achieve excellent sensorless drive performances.

II. Saliency-based Sensorless Drive Feasibility

A. Basic principle of saliency-based sensorless control

In an IPMSM, permanent magnets (PMs) have an effect on not only induced BEMF, but spatial saliency distribution. Non-uniformly positioned PM in the rotor causes a discrepancy between the *d* and *q*-axis reluctance. This result brings about the spatial saliency. Therefore, with a high-frequency signal injection method, the position of the rotor can be estimated based on the saliency. As shown in Fig. 1, if the voltage injection angle is 0 degree when the voltage is injected on the *d*-axis, the *d*-axis self-inductance has a minimum value and the *d*, *q*-axis mutual-inductance must be zero-crossing. Thus, the rotor position can be estimated by measuring variation of the inductance or the current response.

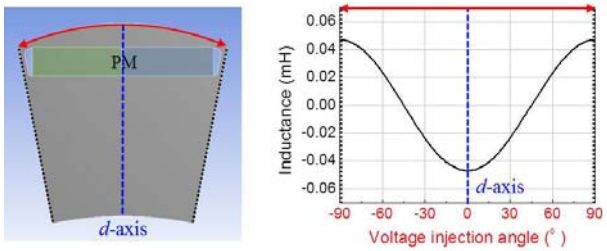

Fig. 1. *d*-axis inductance waveform with high-frequency voltage injection

B. Method1: Contour of inductance and estimation error

However, the inductance waveforms or current responses are distorted with the rotor position by saturation of the core or the cross-saturation effect. Thus, a certain simulation process has to be carried out to estimate rotor position.

1) Nonlinear finite element analysis (FEA) is conducted including PMs to consider the saturation of the core under the load conditions.

2) The next step involves fixing the permeability at each mesh decided in the first step, converting the residual induction of the PM to 0, and performing linear FEA by applying the unit current to the coil of a single phase.

3) The self- and 3-phase mutual- inductances can be obtained as linkage flux per unit current.

4) The procedure is iterated with the rotor position for one

period in the electrical angle.

5) The *d*, *q*-axis self- and mutual-inductances can be calculated via axis transformation.

6) The contour plot of the *d*, *q*-axis mutual-inductances to estimate rotor position is obtained [5].

Consequently, sensorless drive feasibility is predicted by contour plotting zero-crossing of the *d*, *q*-axis mutual-inductances varied with rotor position [3].

C. Method2: Inductance harmonics and estimation error

The effect of the inductance harmonics on the estimation error can be examined mathematically. Each harmonic term of the 3-phase inductance can be transformed into the *d*, *q*-axis inductance using transfer matrix [6]. As a result, the *d*, *q*-axis inductance caused by the *n*-th harmonic of the phase inductance, L^r_{dqh}, can be obtained.

$$L^r_{dqh} = \frac{3}{2} L_h \begin{bmatrix} \cos 6\theta_r m & -\sin 6\theta_r m \\ -\sin 6\theta_r m & -\cos 6\theta_r m \end{bmatrix} \quad @ \ n = 3m-1$$

$$L^r_{dqh} = \frac{3}{2} L_h \begin{bmatrix} \cos 6\theta_r m & \sin 6\theta_r m \\ \sin 6\theta_r m & -\cos 6\theta_r m \end{bmatrix} \quad @ \ n = 3m+1 \quad (1)$$

$$L^r_{dqh} = 0 \quad @ \ n = 3m$$

TABLE I
RELATION BETWEEN THE HARMONIC ORDERS OF THE PHASE INDUCTANCES AND THE D,Q-AXIS MUTUAL-INDUCTANCES

n	2	4	5	7	8	10	11	13	…
m	1	1	2	2	3	3	4	4	…
L_{dqh}	6	6	12	12	18	18	24	24	6*k*-th

where *m* is natural number. *n* is the harmonic order of the phase inductances, and L_h is the magnitude of the *n*-th harmonic. As described in (1), the harmonics of the phase inductances, except the 3*k*-th harmonic terms, cause the 6*k*-th periodic ripple of the *d*, *q*-axis inductances varied with the rotor position during one period in electrical angle (*k*=1, 2, 3…). The relation between the harmonics of the phase inductances and the *d*, *q*-axis inductances can be organized simply as Table I. Therefore, the magnitude of the estimation error is represented by examining the THD of the phase inductances excluding the 3*k*-th harmonic terms (THD_L).

III. Analysis of Design Parameters and Future Work

The configurations of the IPMSMs applied with the design parameters are shown in Fig. 2, and the analysis result of an initial model by using the proposed methods is shown in Fig. 3.

In the full paper, one of the optimal design parameters will be selected based on the analysis results of all the models, and it will be applied to the initial model to reduce the estimation error. Lastly, validity of the estimation methods and the design result will be verified by experiments of the designed IPMSM.

Acknowledgment

This research was supported by the MKE (The Ministry of Knowledge Economy), Korea, under the CITRC (Convergence Information Technology Research Center) support program (NIPA-2013-H0401-13-1008) supervised by the NIPA (National IT Industry Promotion Agency).

This work supported by a research program (The Specialized Research Center on the Future Ground System) funded by the Agency for Defense Development of Korea and we appreciate it.

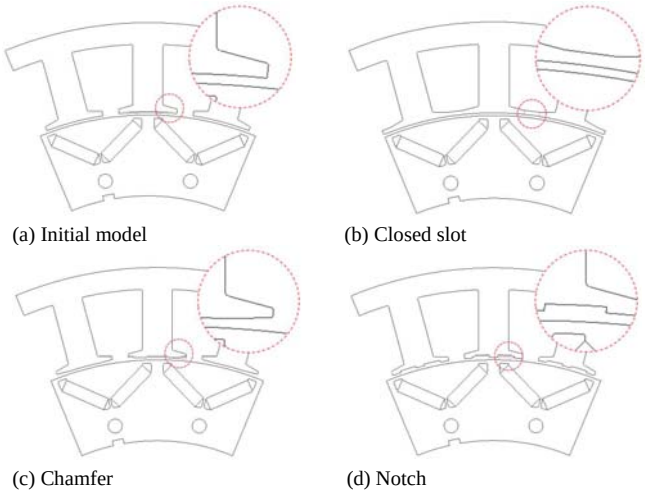

Fig. 2. Configuration of the 115Nm-14kW analysis models

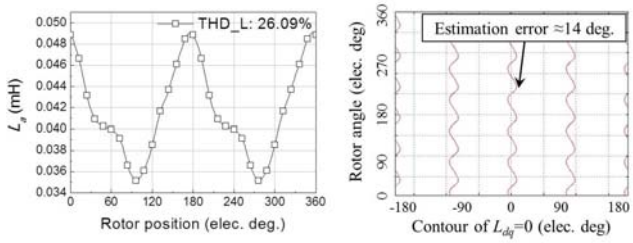

Fig. 3. One-phase self-inductance varied with the rotor position, and the estimated rotor position of the initial model

References

[1] S. Sayeef, G. Foo, and M. F. Rahman, "Rotor Position and Speed Estimation of a Variable Structure Direct-Torque-Controlled IPM Synchronous Motor Drive at Very Low Speeds Including Standstill," *IEEE Trans. Ind. Electron.*, vol. 57, No. 11, pp. 3715-3723, 2010.

[2] Y. Kano, T. Kosaka, N. Matsui and M. Fujitsuna, "Sensorless-oriented design of concentrated winding IPM motors for HEV drive application," *in conf. Rec. IEEE ICEM*, pp. 2709-2715, 2012.

[3] Z. Q. Zhu, Y. Li, D. Howe and C. M. Bingham, "Compensation for rotor position estimation error due to cross-coupling magnetic saturation in signal injection based sensorless control of PM brushless AC motor," *in conf. Rec. IEEE IEMDC*, pp. 208-213, 2007.

[4] R. Wrobel, A. S. Budden, D. Salt, D. Holliday, P. H. Mellor, A. Dinu, P. Sangha, and M. Holme, "Rotor Design for Sensorless Position Estimation in Permanent-Magnet Machine," *IEEE Trans. Ind. Electron.*, vol. 58, No. 9, pp. 3815-3824, 2010.

[5] P. Sergeant, F. De Belie, and J. Melkebeek, "Rotor Geometry Design of Interior PMSMs With and Without Flux Barriers for More Accurate Sensorless Control," *IEEE Trans. Ind. Electron.*, vol. 59, No. 6, pp. 2457-2465, 2011.

[6] M. S. Lim, S. H. Chai, and J. P. Hong, "Design and iron loss analysis of sensorless-controlled interior permanent magnet synchronous motors with concentrated winding," *IET Electric Power Applications*, vol. 8, No. 9, pp. 349-356, 2014.